IJC Heart & Vasculature 51 (2024) 101335

Contents lists available at ScienceDirect

IJC Heart & Vasculature

journal homepage: www.sciencedirect.com/journal/ijc-heart-and-vasculature

Uncovering hub genes and immunological characteristics for heart failure utilizing RRA, WGCNA and Machine learning

Dingyuan Tu [a,b,1], Qiang Xu [c,1], Xiaoli Zuo [b,*], Chaoqun Ma [a,*]

[a] Cardiovascular Research Institute and Department of Cardiology, General Hospital of Northern Theater Command, State Key Laboratory of Frigid Zone Cardiovascular Diseases (SKLFZCD), Shenyang, 110000 Liaoning, China
[b] Department of Cardiology, The 961st Hospital of Joint Logistic Support Force of PLA, 71 Youzheng Road, Qiqihar, 161000 Heilongjiang, China
[c] Department of Cardiology, Navy 905 Hospital, Naval Medical University, 1328 Huashan Road, Changning District, Shanghai 200052, China

ARTICLE INFO

Keywords:
Heart failure
Robust rank aggregation
Weighted gene co-expression network analysis
Machine learning
Immune infiltration

ABSTRACT

Background: Heart failure (HF) is a major public health issue with high mortality and morbidity. This study aimed to find potential diagnostic markers for HF by the combination of bioinformatics analysis and machine learning, as well as analyze the role of immune infiltration in the pathological process of HF.
Methods: The gene expression profiles of 124 HF patients and 135 nonfailing donors (NFDs) were obtained from six datasets in the NCBI Gene Expression Omnibus (GEO) public database. We applied robust rank aggregation (RRA) and weighted gene co-expression network analysis (WGCNA) method to identify critical genes in HF. To discover novel diagnostic markers in HF, three machine learning methods were employed, including best subset regression, regularization technique, and support vector machine-recursive feature elimination (SVM-RFE). Besides, immune infiltration was investigated in HF by single-sample gene set enrichment analysis (ssGSEA).
Results: Combining RRA with WGCNA method, we recognized 39 critical genes associated with HF. Through integrating three machine learning methods, FCN3 and SMOC2 were determined as novel diagnostic markers in HF. Differences in immune infiltration signature were also found between HF patients and NFDs. Moreover, we explored the potential associations between two diagnostic markers and immune response in the pathogenesis of HF.
Conclusions: In summary, FCN3 and SMOC2 can be used as diagnostic markers of HF, and immune infiltration plays an important role in the initiation and progression of HF.

1. Introduction

Heart failure (HF) is a complex clinical syndrome that leads to structural or functional cardiac abnormalities. It is a terminal condition in various cardiovascular diseases and has become a significant public health concern due to the high risk of hospitalization and mortality in these patients [1]. Despite breakthroughs in the understanding of HF etiopathogenesis, the physiopathology that triggers the disease is still not completely understood. Therefore, it is crucial to explore novel biomarkers to improve the accuracy of diagnosis and prognosis in HF patients.

At present, with the wide use of microarray and high-throughput sequencing technology, integrated bioinformatics analyses have showed significant advantages in exploring the pathogenesis and potential treatments for various diseases [2]. Compared to the conventional methods of differential expression analysis, weighted gene co-expression network analysis (WGCNA) has been recognized as an effective method used to identifying key hub genes within modules related to phenotypic traits [3]. In addition, small sample size is a concern with many current microarray datasets, and batch effect has presented grand challenges to the integrative analyses across multiple datasets. In this context, the robust rank aggregation (RRA) method, which can identify the overlapping genes among ranked gene lists, has been utilized in various studies to obtain stable biomarkers [4].

In recent years, an increasing number of studies have demonstrated that immunological dysregulation and deterioration of cardiac function are two interdependent phenomena. Single-cell RNA-sequencing technology has revealed a significant difference in immune cell components

* Corresponding authors.
E-mail addresses: 46357368@qq.com (X. Zuo), xn173760529@foxmail.com (C. Ma).
[1] These authors contributed equally to this work.

https://doi.org/10.1016/j.ijcha.2024.101335
Received 18 November 2023; Received in revised form 24 December 2023; Accepted 2 January 2024

between healthy and failing hearts [5]. Therefore, a comprehensive analysis of the relationship between immune infiltration and HF may provide new references for the diagnosis and treatment of HF.

By utilizing RRA, WGCNA and three machine learning methods, we identified hub genes of HF and constructed a diagnostic model for HF. Additionally, we investigated the interaction between immune infiltration and the hub genes of HF. This work provides new insights into the deep exploration of molecular mechanism involved in HF development.

2. Materials and methods

2.1. Inclusion criteria for datasets

Publically available HF microarray datasets were obtained from the NCBI Gene Expression Omnibus (GEO) database (https://www.ncbi.nlm.nih.gov/geo/). The search results and relevant datasets were filtrated according to the following eligibility criteria: (i) the organism was set as "Homo sapiens"; (ii) datasets within GEO were filtered by "Expression profiling by array"; (iii) the experiments were performed with heart samples of HF patients and NFDs, with a minimum of three samples investigated. Based on these criteria, six datasets were included in our study: GSE16499 [6], GSE26887 [7], GSE42955 [8], GSE57338 [9], GSE76701 [10], and GSE79962 [11]. The series matrix files of these datasets and their corresponding platform files were downloaded as CSV files from GEO. In addition, GSE116250 [12] was selected as the external validation dataset, which includes 50 HF patients (13 with ischemic cardiomyopathy and 37 with dilated cardiomyopathy) and 14 NFDs.

2.2. Identification of differentially expressed genes (DEGs) by RRA method

The six raw datasets were processed using the Bioconductor package limma [13], which included column normalization and log-transformation. Next, DEGs were analyzed by the limma package, and the ranked lists of both upregulated and downregulated DEGs in each dataset were generated based on their fold changes. Finally, we utilized the RRA method-based R package "RobustRankAggreg" to integrate the results of those six datasets to find the most significant DEGs. Genes with an absorbance fold change (logFC) > 1 and adjusted p-value < 0.05 were chosen as significantly DEGs in the RRA analysis.

2.3. Construction of weighted gene co-expression network analysis

Before merging the six microarray datasets, we corrected for batch effects using ComBat from the sva package in order to minimize experimental variance prior to subsequent analysis. Principal component analysis (PCA) was assessed before and after correction and then presented as 2D PCA plots. The final merged dataset had 259 samples with 124 HF patients (64 with ischemic cardiomyopathy and 60 with dilated cardiomyopathy) and 135 NFDs.

To explore the gene interactions, we employed a systems biology approach called WGCNA using the WGCNA R package on the final merged dataset. Firstly, we selected genes with the top 25 % variation across samples in the integrated dataset for WGCNA, ensuring the heterogeneity and accuracy of bioinformatics statistics for further co-expression network analysis. Secondly, genes with a height value > 60 were considered outlier and excluded. Thirdly, we calculated the adjacency matrix from the soft thresholding power β and then converted it into a topological overlap matrix (TOM). Fourthly, using the TOM-based dissimilarity measure, we divided genes into different modules through hierarchical clustering and dynamic tree cutting. Subsequently, modules with highly correlated eigengenes were merged with a merge height of 0.2. Lastly, we defined key genes based on gene significance (GS) and module membership (MM) within the target modules. The intersection of the genes identified through the RRA and WGCNA methods was considered as critical genes in HF.

2.4. Enrichment analysis of critical genes

To further investigate the functional and pathway enrichment of the critical genes in HF, Gene Ontology (GO) and Disease Ontology (DO) enrichment analyses were carried out with the R package "clusterprofiler" [14]. Moreover, pathway enrichment analysis of critical genes was performed using Gene Set Enrichment Analysis (GSEA) based on Kyoto Encyclopedia of Genes and Genomes (KEGG) pathways, and "c2.cp.kegg.v7.4.entrez.gmt" was selected as the reference gene set. Adjusted p-value < 0.05 were considered statistically significant enrichment.

2.5. Screening diagnostic markers by machine learning

In order to determine the diagnostic markers of critical genes for HF, three feature selection methods of machine learning were employed. The procedure is outlined as follows. Firstly, in order to prevent model overfitting, the final merged dataset was divided into the training dataset and internal validation dataset at a ratio of 7:3 with the same percentage of HF patients, and ten-fold cross-validation was employed. Secondly, we used the best subset regression method to identify the feature subset that exhibited optimal classification performance with the "leaps" R package. Additionally, regularization techniques (ridge, elastic net and lasso) were applied to detect the genes that contributed the most to the diagnosis of HF using the "glmnet" R package. All three models were established on the training dataset, and model performance was evaluated by the root mean squared error (RMSE) in the internal validation dataset. Genes from the model with the best performance were selected. Furthermore, the support vector machine-recursive feature elimination (SVM-RFE) method from R package "mlbench" was adopted for classification analysis of the selected biomarkers in the diagnosis of HF. Finally, the intersection of best subset regression, SVM-RFE and the best performing model of regularization technique were considered as potential diagnostic markers of HF.

2.6. Construction and verification of a diagnostic model of HF

After obtaining the diagnostic markers, a diagnostic model for HF was constructed by fitting these genes into a binary logistic regression model using the "glm" R package. The model was then visualized using a nomogram generated from the "rms" R package. The discriminatory capability of the model was evaluated using the receiver operating characteristic (ROC) curve, while its calibration was assessed using a calibration plot. The calibration plot was generated from the "givitiR" R package. This evaluation process was performed in both the final merged dataset and external validation dataset.

2.7. Immune infiltration analysis

To evaluate the immune activities involved in HF, we employed single-sample gene set enrichment analysis (ssGSEA) to investigate the varying degrees of infiltration of 29 immune signatures in HF patients and NFDs. Furthermore, we generated a correlation heatmap using the "corrplot" R package to illustrate the correlation between 16 immune cell types and 13 immune-related functions. Additionally, we used "ggplot2" R package to perform PCA clustering analysis on immune infiltration matrix data and generate a two-dimensional PCA clustering map. Lastly, ssGSEA scores were plotted by "ggplot2" R package to compare and visualize the levels of these immune signatures between HF patients and NFDs.

2.8. Correlation analysis between diagnostic markers and immune infiltration in HF

In order to investigate the role for diagnostic markers in modulating

HF immune infiltration, we established relationships between diagnostic markers and immune signatures in 50 HF samples of the external validation dataset. Besides, correlation analyses were performed between diagnostic markers and other genes, and genes with an absolute correlation coefficient greater than 0.5 and a p-value less than 0.05 were defined as diagnostic markers-related genes. To further explore the potential role of the diagnostic markers, KEGG pathway enrichment analyses of these diagnostic markers-related genes were performed by R package "clusterProfiler".

2.9. Statistical analysis

Independent two-sample t-tests were applied to identify DEGs between samples of HF patients and NFDs if the data were normally distributed and had equal variance; otherwise, Mann–Whitney nonparametric tests were used. P-values were adjusted for multiple testing by the Benjamini Hochberg method, and all P-values were based on two-tailed statistical analysis. Genes with an absorbance fold change (logFC) > 1 and an adjusted p-value < 0.05 were considered significantly differentially expressed. Pearson correlation coefficient was calculated when variables were normally distributed, while Spearman rank correlation was used otherwise. Correlation coefficients were interpreted as follows: values 0 to 0.3 (0 to −0.3) indicating negligible correlation, 0.3 to 0.5 (−0.3 to −0.5) indicating low positive (negative) correlation, 0.5 to 0.7 (−0.5 to −0.7) indicating moderate positive (negative) correlation, 0.7 to 0.9 (−0.7 to −0.9) indicating high positive (negative) correlation and 0.9 to 1 (−0.9 to −1) indicating very high positive (negative) correlation [15]. All data analyses in the present study were performed using R (version 4.1.2) and Rstudio (version 2021.09.1).

3. Results

3.1. Identification of significant DEGs by the RRA method

Fig. 1 depicts a flow diagram of our study. The sample characteristics of these included datasets are summarized in Supplementary Table 1, including Dataset ID, study country, number of HF patients and NFDs and platform ID. Based on the results of DEGs analysis in each dataset (Fig. 2A-2F), a total of 58 up-regulated and 41 down-regulated significant DEGs were identified by the RRA method. The top 20 up-regulated

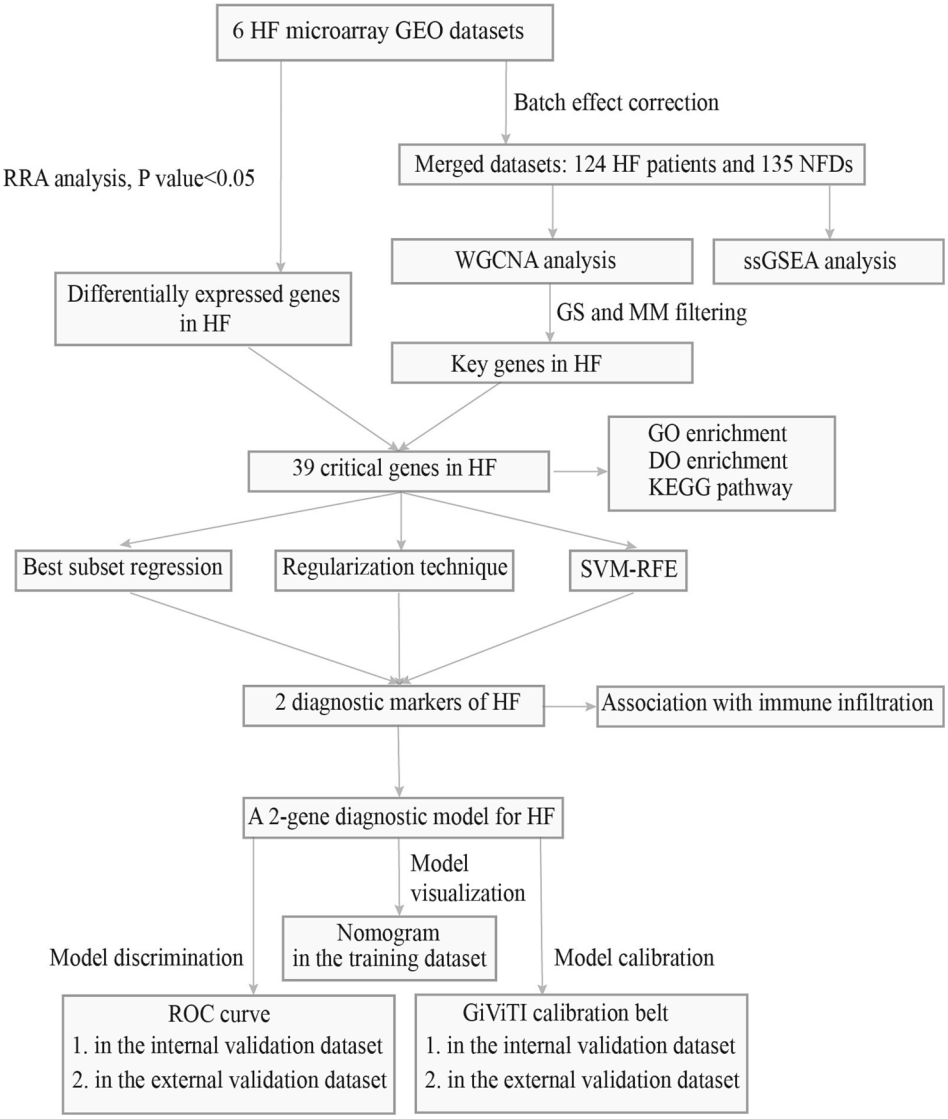

Fig. 1. Study workflow. Abbreviations: HF, heart failure; GEO, gene expression omnibus; RRA, robust rank aggregation; NFDs, nonfailing donors; WGCNA, weighted gene co-expression network analysis; ssGSEA, single-sample gene set enrichment analysis; GS, gene significance; MM, module membership; GO, Gene Ontology; DO, Disease Ontology; KEGG, Kyoto Encyclopedia of Genes and Genomes; SVM-RFE, support vector machine-recursive feature elimination; ROC, receiver operating characteristic.

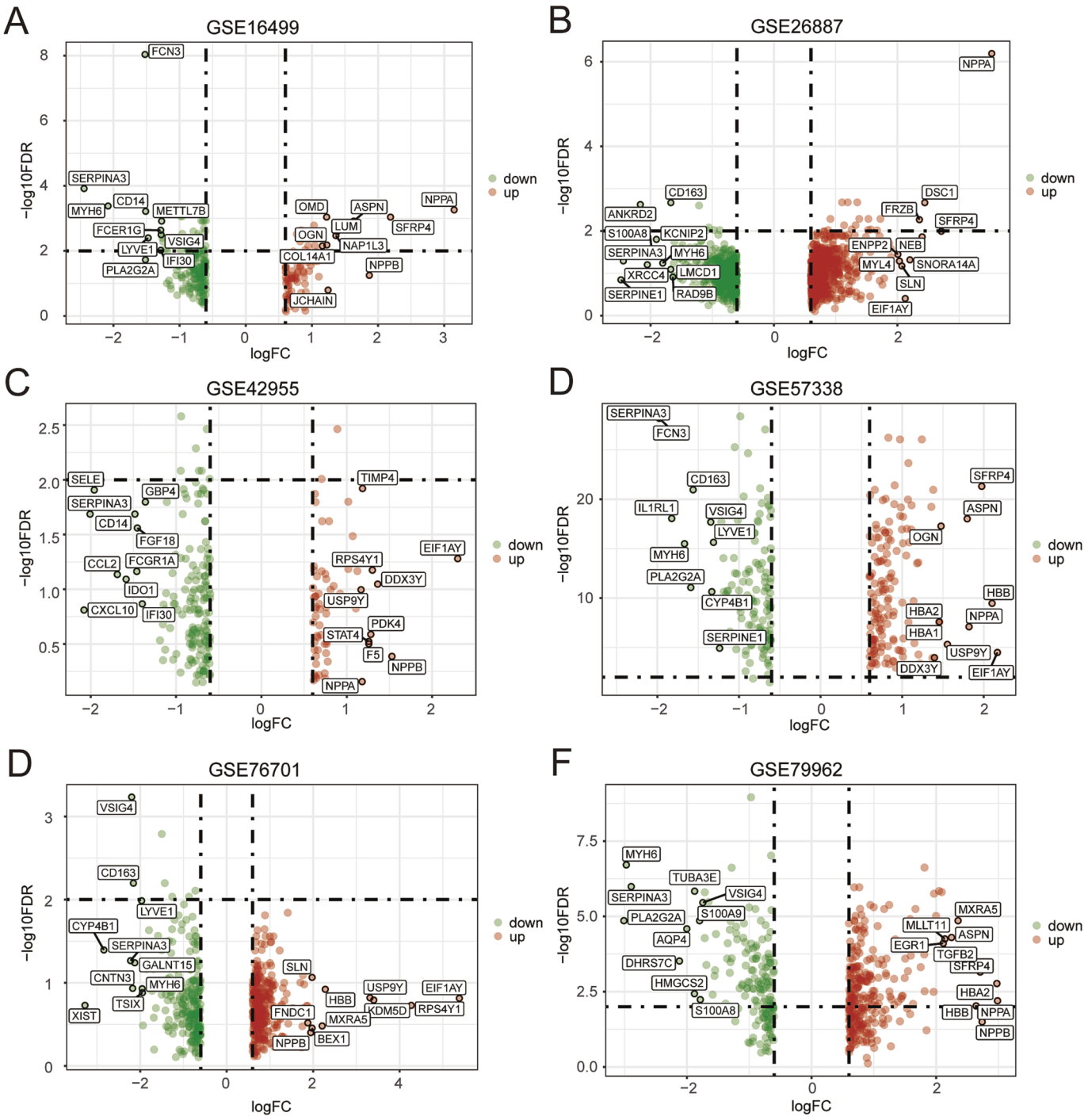

Fig. 2. Volcano plot of differentially expressed genes in cardiac tissues between HF patients and NFDs. Significant upregulated genes are shown in red (HF patients vs. NFDs), downregulated genes in green (HF patients vs. NFDs). The 10 most significantly differentially expressed genes are shown in the boxes. **A** GSE16499. **B** GSE26887. **C** GSE42955. **D** GSE57338. **E** GSE76701. **F** GSE79962. Abbreviations: HF, heart failure; NFDs, nonfailing donors. (For interpretation of the references to color in this figure legend, the reader is referred to the web version of this article.)

and down-regulated DEGs are shown in the heatmap (Fig. 3).

3.2. *Identification of gene co-expression networks and modules*

The merged gene expression matrix of six datasets was presented in a two-dimensional PCA cluster diagram before and after removal of batch effect (Fig. 4A-4B). The results showed that batch effect between different datasets was less obvious after normalization and batch effect adjustment, indicating that the final merged dataset can be used in subsequent analysis.

To find the key modules most associated with HF, we constructed the WGCNA network on the final merged dataset using the "WGCNA" R package. The dendrogram and traits of all samples were illustrated in Fig. 5A, and when the soft threshold power was set as fourteen, the scale-free R2 was 0.862 to obtain a highest average connectivity degree (Fig. 5B). Similar modules with a height cut-off value of 0.2 were merged (Fig. 5C), and 6 modules marked in turquoise, red, yellow, blue, brown and gray were identified using the dynamic branch-cutting approach (Fig. 5D). Through the heatmap of module–trait correlations, we found that the yellow module ($r = 0.75$; $p < 0.0001$) was the most highly

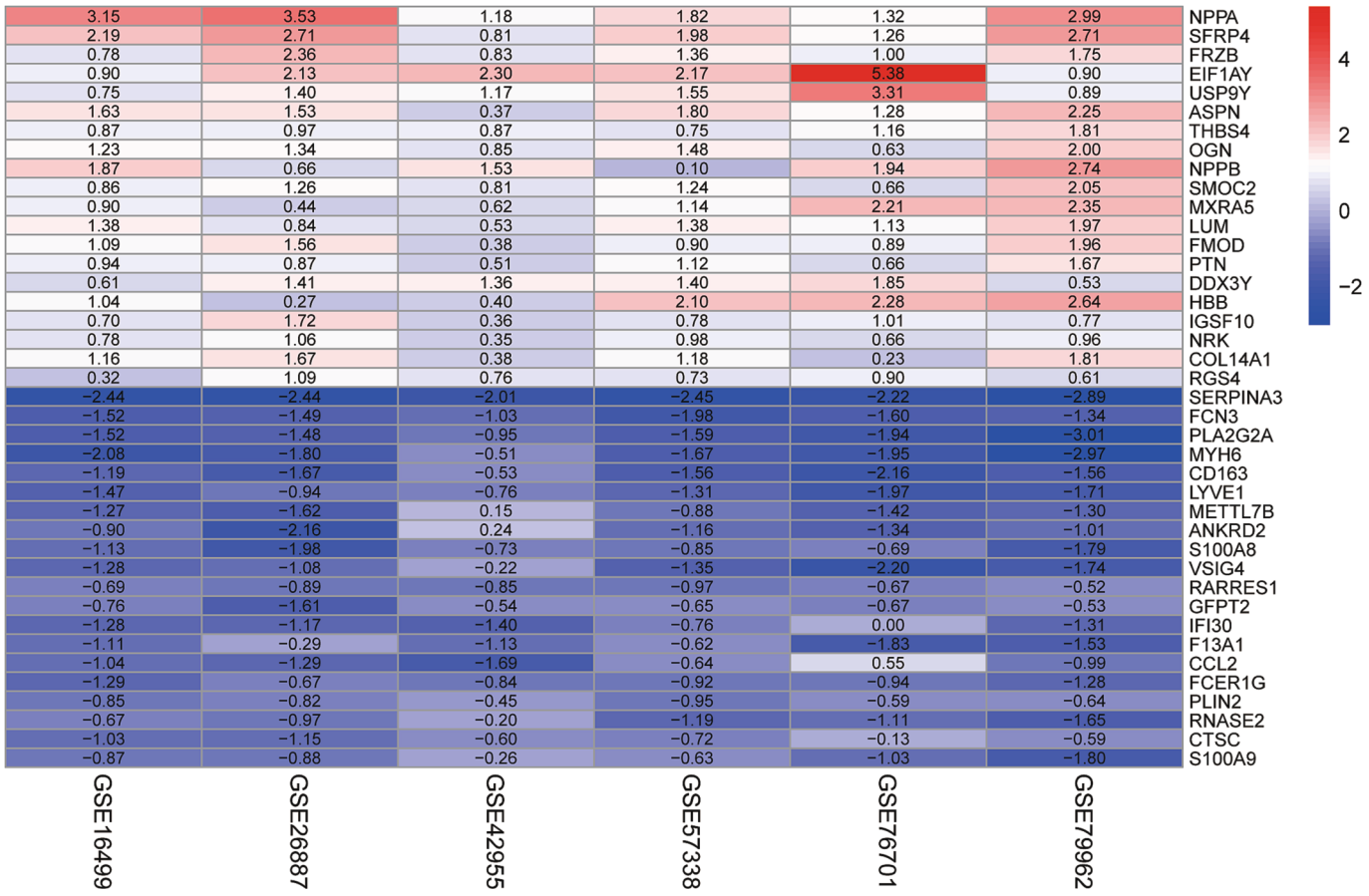

Fig. 3. Heatmap of the top 20 upregulated and the top 20 downregulated genes from RRA analysis of six datasets. Each column represents one dataset and each row indicates one gene. The white color ranging from red to blue represents the changing process from up- to down-regulation (HF patients vs. NFDs.) The number in each rectangle represents the value of log2 (fold change). The red color represents up-regulation while blue color represents down-regulation. The number in each rectangle represents the value of log2 (fold change) in each dataset calculated by the "limma" R package. Abbreviations: RRA, Robust Rank Aggregation; HF, heart failure; NFDs, nonfailing donors. (For interpretation of the references to color in this figure legend, the reader is referred to the web version of this article.)

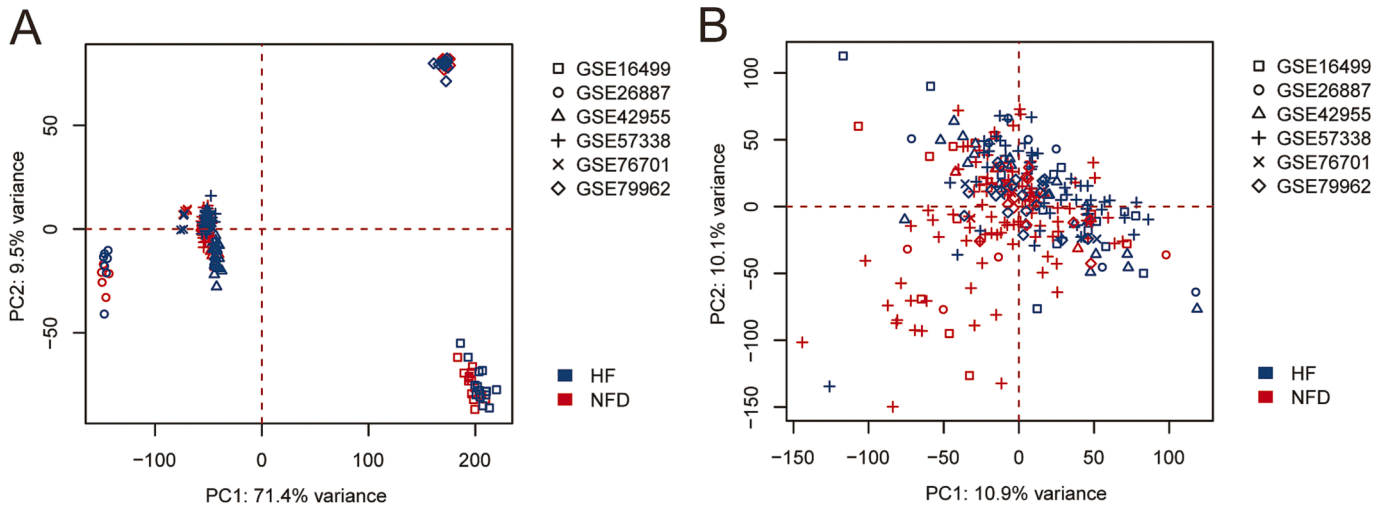

Fig. 4. Two-dimensional PCA cluster plot before and after batch effect correction. **A** Before normalization. **B** After normalization. Abbreviations: PCA, Principal Component Analysis.

correlated module with HF (Fig. 5E), which was considered as key module for HF. After calculating correlation between GS and MM in the yellow module, significant correlations between GS and MM ($r = 0.58$; $p < 0.0001$) for HF in the yellow module are presented in Fig. 5F. The yellow module contained a total of 211 genes. 39 genes from the intersection between the RRA and WGCNA method is considered as critical genes in HF and retained for further analysis (Fig. 5G).

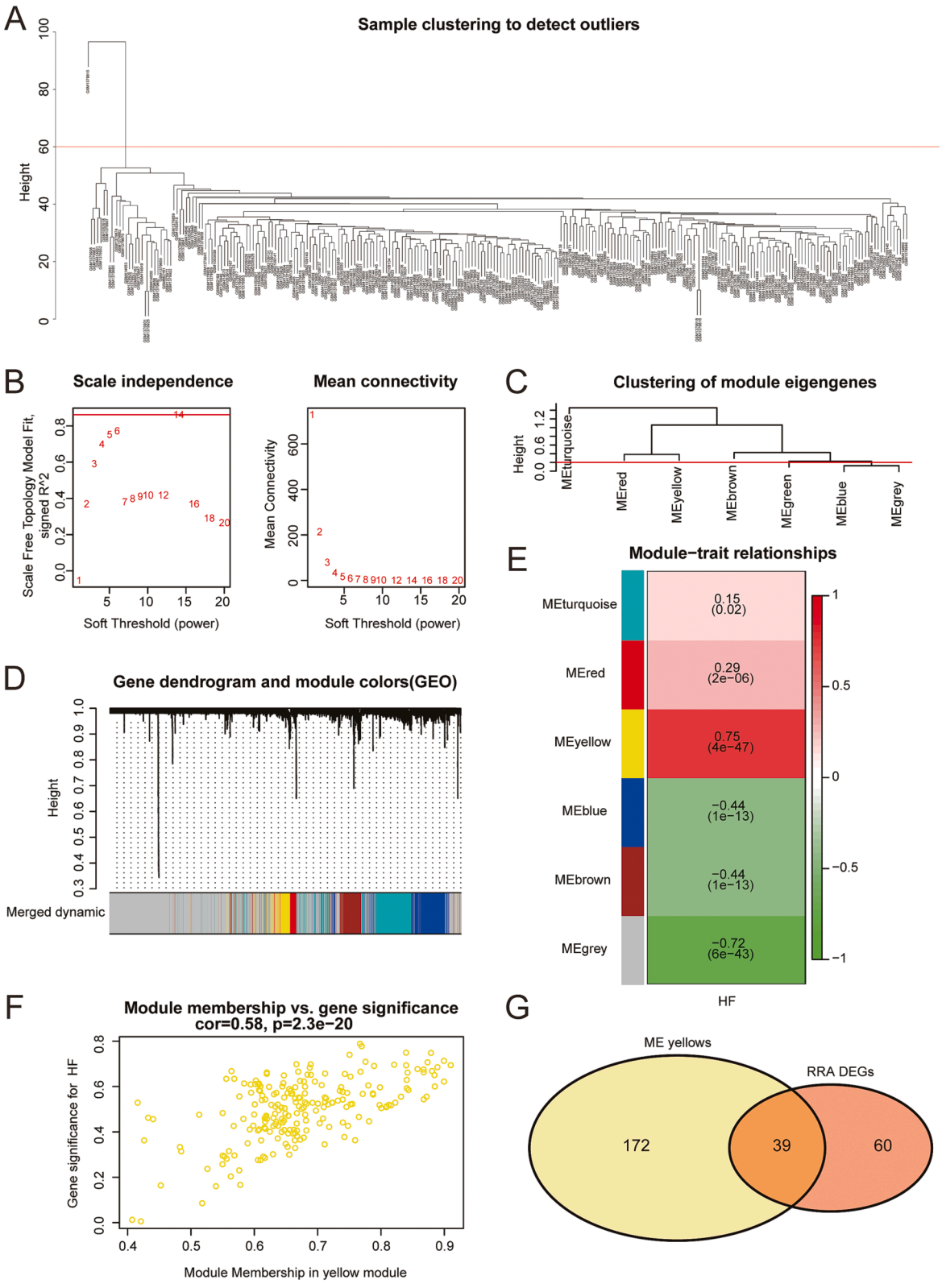

Fig. 5. Weighted gene co-expression network analysis. **A** Sample clustering to detect outliers in the merged dataset. **B** Analysis of the scale-free topology index and mean connectivity by setting unequal soft-thresholding power between 1 and 20. **C** Clustering of module eigengenes. The red line indicates cut height (0.2). **D** Hierarchical cluster dendrogram of all DEGs based on one dissimilarity measure (1-TOM). **E** Heatmap of the correlation between module eigengenes and clinical phenotypes. The yellow module was significantly correlated with HF. **F** Correlation plot between module membership (X-axis) and gene significance (Y-axis) of genes contained in the yellow module. **G** Venn diagram showing the intersection of genes between the RRA DEGs and the genes in the yellow module of WGCNA. Abbreviations: DEGs, differentially expressed genes; HF, heart failure; RRA, Robust Rank Aggregation; WGCNA, Weighted gene co-expression network analysis. (For interpretation of the references to color in this figure legend, the reader is referred to the web version of this article.)

3.3. Functional enrichment and pathway analyses of critical genes

GO functional enrichment analysis indicated that the five most enriched GO terms of the critical genes for biological process (BP) were the extracellular matrix organization, extracellular structure organization, external encapsulating structure organization, muscle system process, and positive regulation of inflammatory response. Within the cell component (CC) categories, collagen-containing extracellular matrix, secretory granule membrane, vacuolar lumen, collagen trimer, and platelet alpha granule were dominant terms. Under the molecular function (MF), extracellular matrix structural constituent, glycosaminoglycan binding, sulfur compound binding, heparin binding, and collagen binding were significantly enriched (Fig. 6A). The Disease Ontology (DO) enrichment analysis results are shown in Fig. 6B. Diseases enriched by critical genes mainly included coronary artery disease, arteriosclerosis, atherosclerosis, arteriosclerotic cardiovascular disease, and myocardial infarction. Additionally, GSEA results showed that the enriched pathways mainly involved B cell receptor signaling pathway and natural killer cell mediated cytotoxicity (Fig. 6C).

3.4. Determination of diagnostic markers

To determine the critical diagnostic biomarkers of HF, feature selection was further performed in our study. Under the result of best subset regression, the model of six features (AEBP1, FCN3, MYH6, NPPA, SGPP2, and SMOC2) showed the lowest BIC score (BIC = −216.5151) (Fig. 7A-7B). For the regularization technique, the binomial deviance curve of LASSO regression, ridge regression and elastic net regression was shown in Fig. 7C–7E, and mean squared error was calculated for each α value in the elastic net regression (Supplementary Table 2. The least mean squared error was obtained when the value for α was set at 0.33. By comparing performance of these three models of regularization technique in the internal validation dataset through RMSE, we can obtain the conclusion that LASSO regression is the optimal model (Fig. 7F). In addition, two critical genes were identified using the SVM-RFE algorithm as diagnostic markers (Fig. 7G). With the intersection of best subset regression, LASSO regression and SVM-RFE algorithm, FCN3 and SMOC2 were finally obtained as diagnostic markers of HF (Fig. 7H).

3.5. Construction and validation of the diagnostic model

In order to understand the relationship between the expression of two diagnostic markers and HF, a multivariate logistic regression model was constructed. Forest plot demonstrated that two of the diagnostic markers were independently associated with HF (Fig. 8A), and a nomogram was established based on the logistic regression analysis (Fig. 8B). In the merged dataset, the nomogram yielded an AUC of 0.985 (95 % CI, 0.974–0.996) while in the external validation dataset, the nomogram exhibited an AUC of 0.976 (95 % CI, 0.945–0.999). Of note, the diagnostic accuracy of the nomogram was superior to that of B-type natriuretic peptide (BNP) (Fig. 8C-8D). Furthermore, the GiViTI calibration belt revealed that there was no significant deviations in both datasets (P = 0.236, P = 0.857) (Fig. 8E-8F), indicating that the logistic regression model showed good fit between the predicted and observed probabilities. Meanwhile, the differential expression of FCN3 and SMOC2 was validated in the GSE116250 database, which further demonstrated their diagnostic value for HF (Fig. 8G-8H).

To further illuminate the roles of these two diagnostic markers in HF, Pearson correlation was applied to examine the correlation between the mRNA expression of these markers and left ventricular ejection fraction (LVEF) in 15 HF patients of GSE16499. As showcased in **Supplementary Fig. 1**, the expression of SMOC2 was negatively correlated with LVEF in HF patients, indicating that SMOC2 may be associated with deterioration of cardiac function in HF patients.

3.6. Immune infiltration results

To further identify the immune status between HF patients and NFDs, ssGSEA was used to quantify the infiltrating scores of diverse immune cell subpopulations and immune-related functions. The PCA results showed that there was a notable difference in immune infiltration between HF and NFDs (Fig. 9A-9B). Correlation heatmap of 16 immune cell types indicated that TIL was highly positively related with Macrophages (r = 0.73), Neutrophils (r = 0.82) and T helper cells (r = 0.77). For immune-related functions, the following pairs showed a high positive correlation: APC co inhibition and T cell co inhibition (r = 0.83), parainflammation and inflammation promoting (r = 0.71), parainflammation and CCR (r = 0.84), parainflammation and Check-point (r = 0.78), check-point and APC co stimulation (r = 0.72), check-point and CCR (r = 0.85), check-point and T cell co inhibition (r = 0.78) (Fig. 9C-9D). The bar graph of the immune cell infiltration demonstrated that the score of aDCs, B cells, CD8+ T cells, iDCs, macrophages, mast cells, neutrophils, NK cells, Th1 cells, Th2 cells, TIL, and Treg was significantly different between HF and NFDs. Similarly, there was a different infiltration of immune-related functions in APC co inhibition, checkpoint, cytolytic activity, HLA, inflammation promoting, T cell co inhibition, T cell co stimulation, Type I IFN response between HF patients and NFDs (Fig. 9E-9F).

3.7. Analysis of diagnostic markers and immune infiltration

To further investigate the relationship between diagnostic markers and immune infiltration, the correlations between FCN3, SMOC2 and 29 immune signatures were explored. In terms of immune cells, FCN3 was positively correlated with Treg (r = 0.37) and negatively correlated with aDCs (r = −0.40), as well as mast cells (r = −0.45); while SMOC2 was positively correlated with mast cells (r = 0.49) and negatively correlated with macrophages (r = −0.31). For immune-related functions, FCN3 showed positive correlation with T cell co inhibition (r = 0.53), as well as APC co inhibition (r = 0.45) and negative correlation with Type I IFN response (r = −0.55), inflammation promoting (r = −0.50), HLA (r = −0.43), as well as cytolytic activity (r = −0.36); while SMOC2 showed positive correlation with type I IFN response (r = 0.49), inflammation promoting (r = 0.48), HLA (r = 0.42), as well as cytolytic activity (r = 0.35) and negative correlation with T cell co inhibition (r = −0.48), as well as APC co inhibition (r = −0.43) (Fig. 10A–10D).

In order to further investigate the potential associations between diagnostic markers and immune response in the pathogenesis of HF, we performed GSEA on the HF samples of the external validation dataset. GSEA results showed that the enriched immune-related pathways of FCN3 mainly involved in complement and coagulation cascades, hematopoietic cell lineage, and natural killer cell mediated cytotoxicity. As for SMOC2, Fc epsilon RI signaling pathway, Fc gamma R-mediated phagocytosis, and leukocyte transendothelial migration were meaningful immune-related pathways (Fig. 10E-10F).

4. Discussion

In the present study, we performed an integrated bioinformatics analysis using six publicly available HF microarray datasets (GSE16499, GSE26887, GSE42955, GSE57338, GSE76701, and GSE79962). By combining the RRA with WGCNA method, we identified 39 critical genes in HF. Through integrating three feature selection methods including best subset regression, regularization technique and SVM-RFE, FCN3 and SMOC2 were determined as diagnostic markers in HF. Additionally, ssGSEA analysis was conducted to explore the association between inflammation and HF.

HF is a complex clinical syndrome characterized by impaired cardiac pump function and reduced tissue perfusion and metabolism. Despite the constant advancement in treatment modalities, the mortality of HF is increasing annually, imposing a heavy burden on families and society

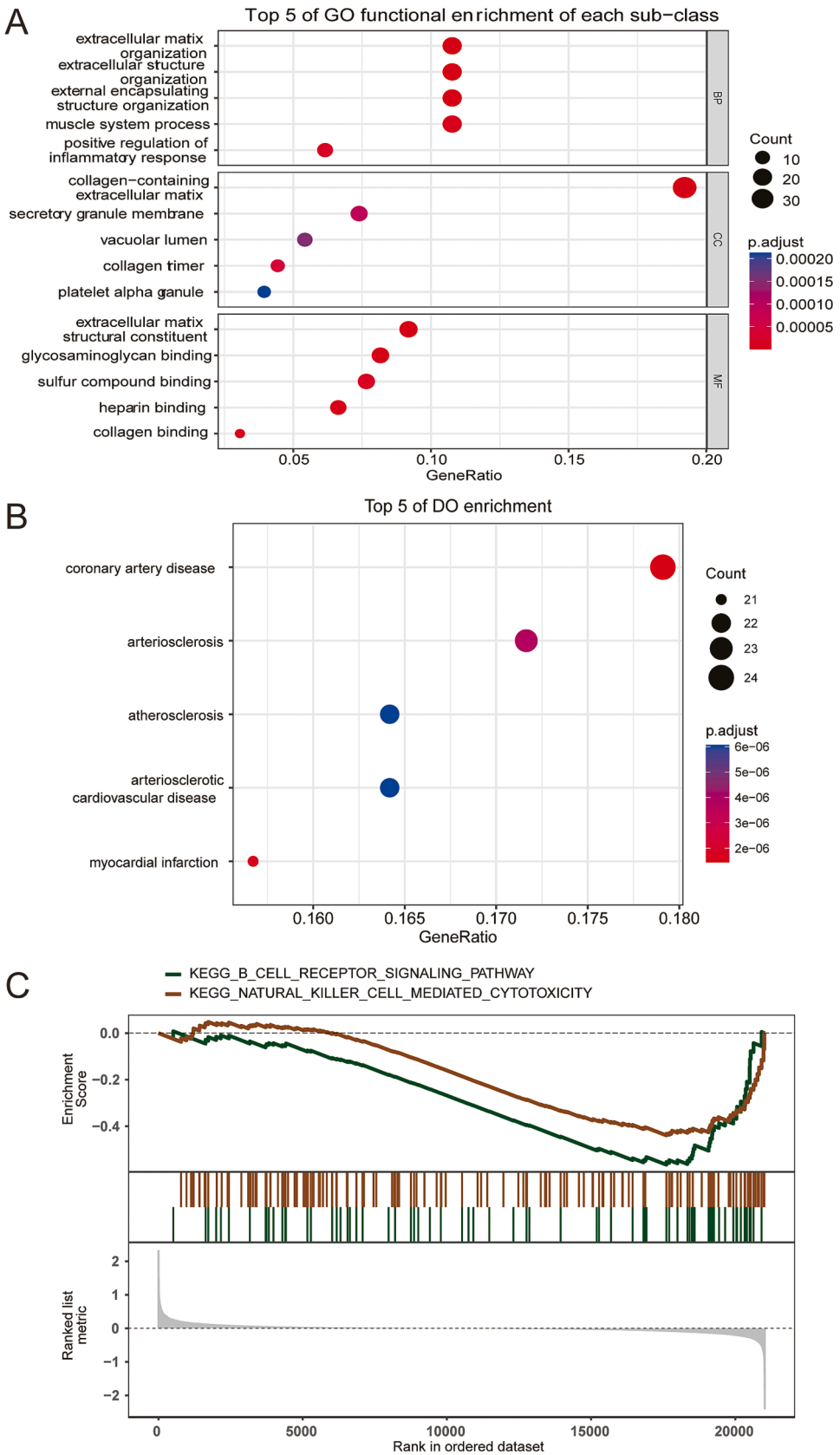

Fig. 6. Enrichment analysis of critical genes. **A** Bubble plot of top 5 enriched GO terms of critical genes in each category. **B** Bubble plot of top 5 enriched DO terms of critical genes. **C** GSEA analysis based on the KEGG pathway database. Abbreviations: GO, Gene Ontology; BP, biological process; CC, cellular components; MF, molecular functions; DO, Disease Ontology; GSEA, Gene Set Enrichment Analysis; KEGG, Kyoto Encyclopedia of Genes and Genomes.

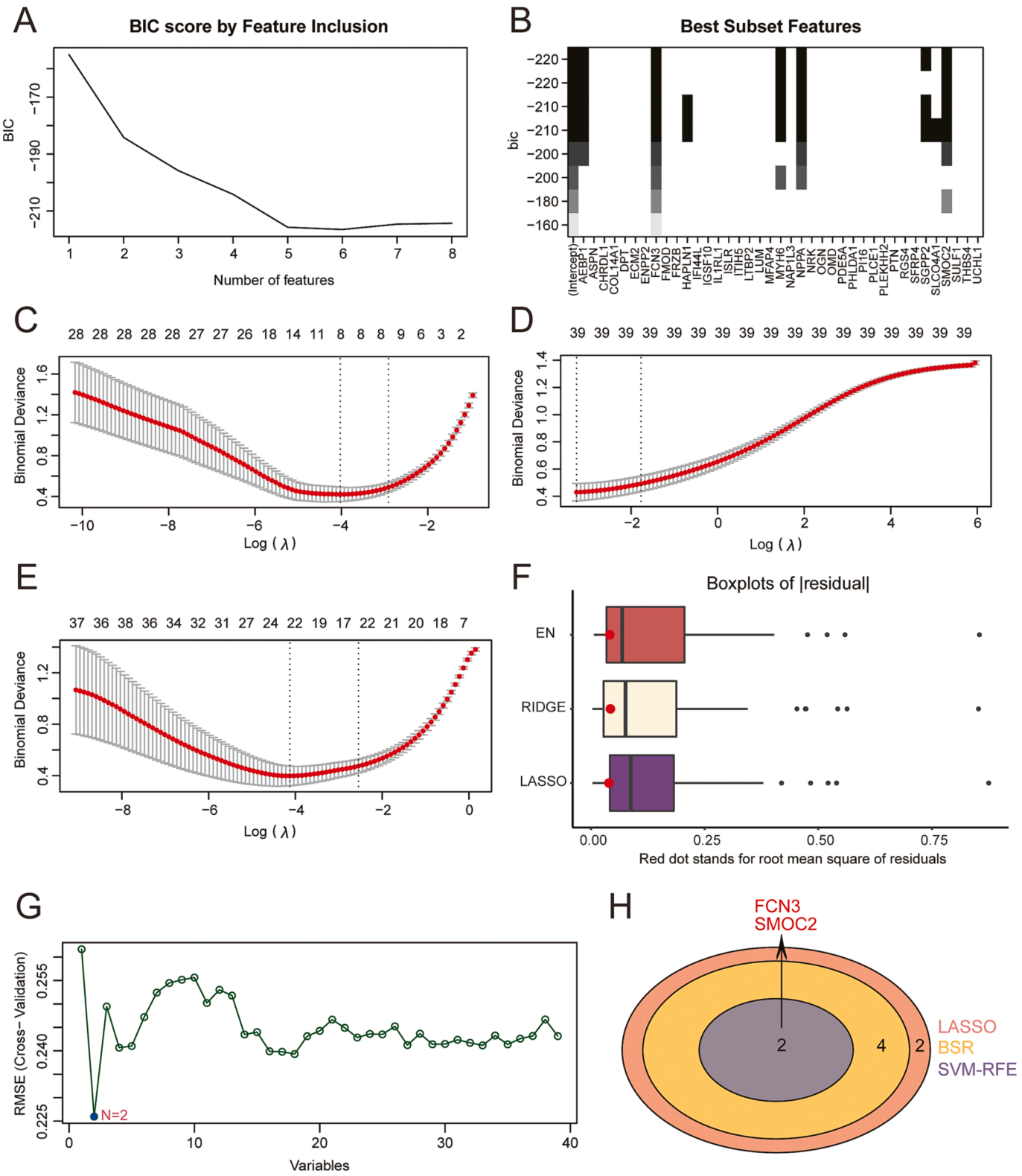

Fig. 7. Machine-learning model to identify diagnostic markers. **A** Bayesian information criterion score by feature inclusion. **B** Model performance based on different feature subsets. **C** LASSO regression algorithm to screen diagnostic markers. **D** Ridge regression algorithm to screen diagnostic markers. **E** Elastic net regression algorithm to screen diagnostic markers. **F** Root mean squared error of three models of regularization technique in the internal validation dataset. Red dot stands for root mean square of residuals. **G** SVM-RFE algorithm to detect diagnostic markers. **H** Venn diagram showing the intersected genes of best subset regression, LASSO regression and SVM-RFE algorithm. Abbreviations: LASSO, least absolute shrinkage and selection operator; SVM-RFE, Support vector machine-recursive feature elimination. (For interpretation of the references to color in this figure legend, the reader is referred to the web version of this article.)

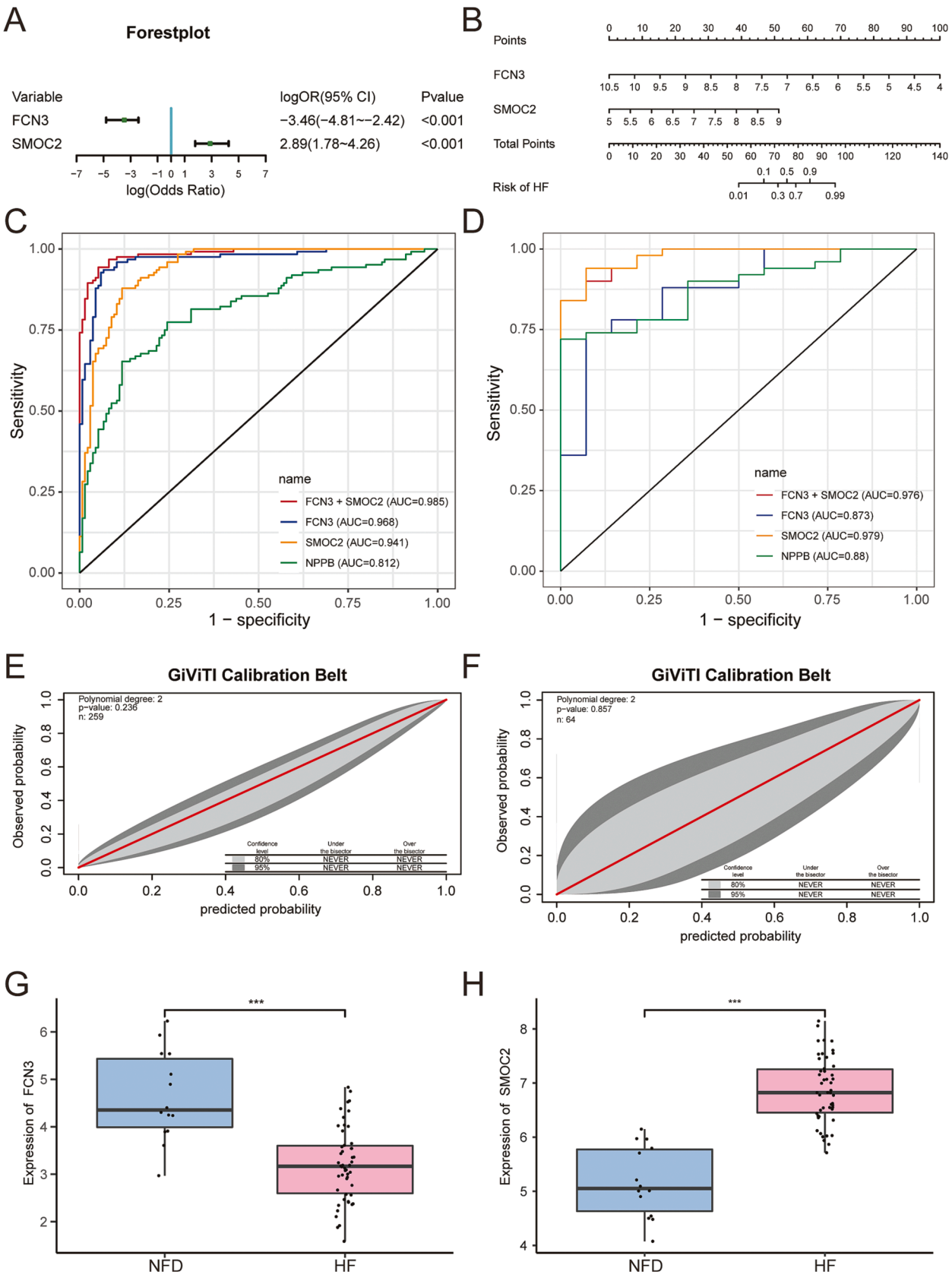

Fig. 8. Development and validation of diagnostic model for HF. **A** Forest plot of FCN3 and SMOC2 in a multivariate logistic regression analysis. **B** Nomogram for the 2-variable prediction model of HF probability. The ROC curve of the nomogram in the merged dataset (**C**) and external validation dataset (**D**). The GiViTi calibration belt of the nomogram in the merged dataset (**E**) and external validation dataset (**F**). The FCN3 (**G**) and SMOC2 (**H**) expression in the external validation dataset. ns: no significance, *p < 0.05, **p < 0.01, ***p < 0.001. Abbreviations: HF, heart failure; ROC, receiver operating characteristic.

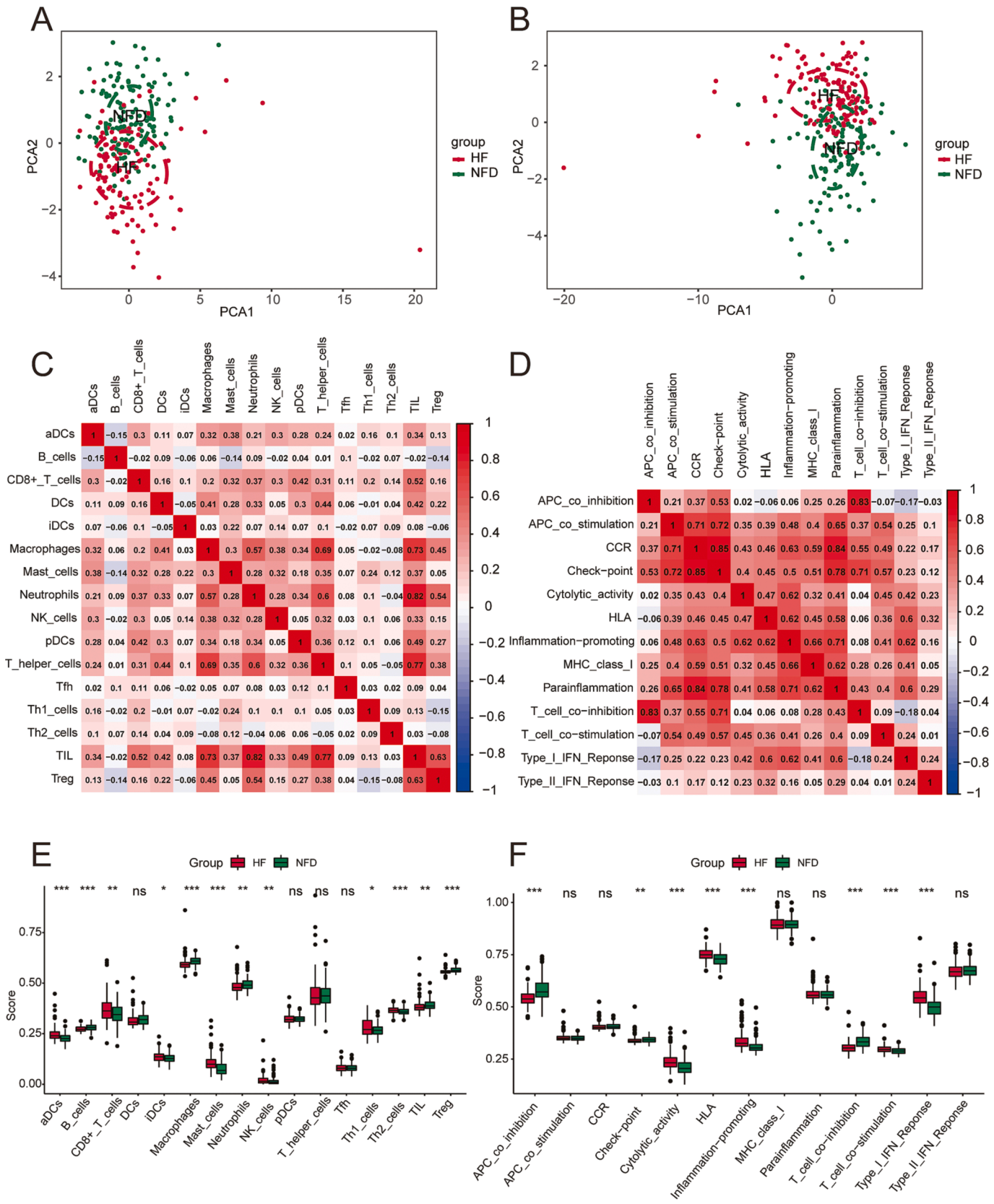

Fig. 9. Evaluation and visualization of immune infiltration in HF. Two-dimensional PCA cluster plot of immune cell (**A**) and immune-related function (**B**) infiltration between cardiac tissues of HF patients and NFDs. Correlation matrix of the immune cell (**C**) and immune-related function (**D**) infiltration. Red indicates positive correlation and blue indicates negative correlation. The darker the color, the stronger the correlation. The scores of immune cells (**E**) and immune-related functions (**F**) between cardiac tissues of HF patients and NFDs. ns: no significance, *p < 0.05, **p < 0.01, ***p < 0.001. Abbreviations: HF, heart failure; PCA, Principal Component Analysis; NFDs, nonfailing donors. (For interpretation of the references to color in this figure legend, the reader is referred to the web version of this article.)

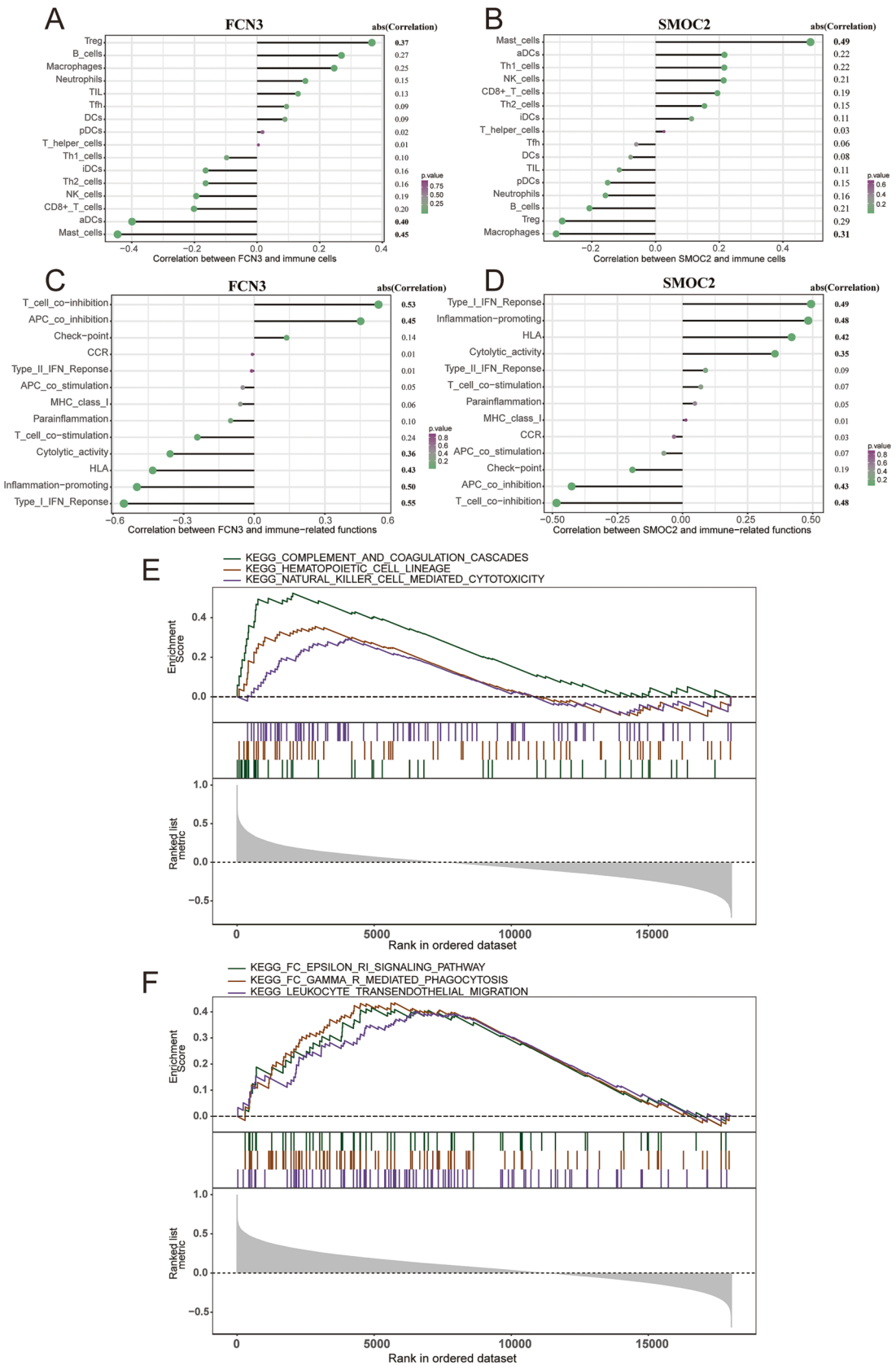

Fig. 10. Association between FCN3, SMOC2 and immune infiltration in HF. Correlation between FCN3 (**A**), SMOC2 (**B**) and immune cell infiltration. Correlation between FCN3 (**C**), SMOC2 (**D**) and immune-related function infiltration. Significant correlations are indicated in bold. Top 3 gene sets (according to GSEA enrichment score) enriched in the HF samples of FCN3 (**E**) and SMOC2 (**F**). Abbreviations: HF, heart failure; GSEA, Gene Set Enrichment Analysis.

[16]. The occurrence and development of HF involve multiple biological mechanisms, such as inflammatory responses, activation of the neuroendocrine system, oxidative stress, and so on. Finding novel molecular biomarkers is essential for clarifying the pathogenesis of HF.

With the advancement of high-throughput sequencing and microarray technology in recent years, integrated bioinformatics methods have emerged as efficient tools for identifying potential biomarkers for the diagnosis, treatment, and prognosis of HF. DEGs analysis is a bioinformatics approach that has been widely and successfully applied for the detection of disease biomarkers. A limitation of the conventional DEGs analysis is that the difference in many genes do not reach statistical significance after correction for multiple tests. In our research, we used the RRA method to address this limitation. This method incorporates the differential expression ranking of each gene across all datasets and performs a hypothesis test based on the ranking vector. The resulting p-value is then used to determine whether the gene has a robust differential expression. Additionally, we employed WGCNA, a widely used method for biological network analysis, to detect coexpression modules and hub genes in HF. It can dissect genes into network modules and find the robust gene modules that are significantly associated with clinical traits. RRA and WGCNA method can complement each other and narrow down potential diagnostic marker candidates. To our knowledge, our study is the first to use RRA combined with WGCNA to explore novel diagnostic markers associated with HF.

As an efficient tool for data mining, machine learning is currently receiving enormous attention and being used in bioinformatics and its related fields. Feature selection is a necessary step for the construction of machine learning models. The greatest advantage of feature selection is to help improving model accuracy and reducing model complexity, as it can remove redundant and irrelevant features to reduce the input dimensionality and help us identify the underlying mechanism that connects gene expression with relevant diseases [17]. In our study, feature selection was performed through best subset regression and three regularization methods: LASSO regression, ridge regression and elastic net. All three models were established on the training dataset and evaluated in the internal validation dataset by the RMSE value, which is a goodness-of-fit indicator. SVM-RFE is another classic feature selection method used in our research. It can rank the genes by training a SVM model and selects critical genes using recursive feature elimination algorithm. With these machine learning models we have determined FCN3 and SMOC2 as diagnostic markers of HF.

In current clinical guidelines, BNP is the gold standard biomarkers for the diagnosis and assessment of HF. Nonetheless, a recent study found that very low BNP levels (<50 pg/ml) were observed in 4.9 % of HF patients, and a small proportion (0.1 % to 1.1 %) had BNP levels even below detection limits [18]. In our established diagnostic model, compared with BNP alone, the combination of FCN3 and SMOC2 had a better diagnostic value and significantly improved the diagnostic accuracy. FCN3 is a glycoprotein which consists of a N-terminal collagen-like domain and a C-terminal fibrinogen-like domain [19]. It can activate the complement system via the lectin pathway, giving rise to both antimicrobial defense and homeostatic balance. Previous studies have shown that the expression of FCN3 in many types of cancerous tissues was significantly decreased such as squamous cell lung carcinoma [20], hepatocellular carcinomas [21], and ovarian cancer [22]. In addition, the expression level of FCN3 has a certain connection with cardiovascular diseases. Lower FCN3 serum levels were observed in rheumatic heart disease patients when compared to controls [23], while increased FCN3 levels were observed in abdominal aortic aneurysm patients' plasma, suggesting it is associated with the presence and progression of abdominal aortic aneurysm [24]. SMOC2, which is a secreted, matricellular protein, belongs to the SPARC/osteonectin/BM40 family proteins. It is involved in various pathophysiological processes such as angiogenesis, tumorigenesis, tissue fibrosis and calcification [25–27]. Silencing of SMOC2 expression slows the progression of renal failure by repressing fibroblast to myofibroblast differentiation through inhibition of multiple cellular signaling pathways including MAPKs, Smad, and Akt [28]. Besides, SMOC2 can act as an inhibitor of calcification and mineralization. Endogenous SMOC2 can stimulate bone healing and attenuate age-related bone loss [29].

Systemic inflammation has been recognized as a common pathobiologic characteristic of HF. To further investigate the role of immune infiltration in HF, we conducted ssGSEA to quantify the immune infiltration based on 16 immune cell types and 13 immune-related functions. The results showed that seven immune cells (aDCs, CD8+ T cells, iDCs, Mast cells, NK cells, Th1 cells, and Th2 cells) infiltrated higher in HF group. Single-cell RNA sequencing from recent studies revealed that the majority innate immune cell subpopulations, including mast cells, monocytes and macrophages, neutrophils, DCs, and NK cells underwent extensive activation in pressure overload-induced HF in mice [5]. Previous studies have found that in the myocardial infarction (MI) model of mice, activation of cytotoxic CD8+ T cells by DCs contributes to aggravation of post-ischemic inflammatory damage of the myocardium and corresponding decreased cardiac function [30]. Furthermore, Ngkelo et al. [31] found that mast cells accumulate in the heart at day 7 after MI, and mast cells can improve cardiomyocyte contractility via alteration of PKA-regulated force-Ca2+ interactions in response to post-MI HF mice. Conversely, the score of B cells, Macrophages, Neutrophils, TIL, and Treg was lower in HF group. In mouse models of HF, induction of neutropenia could reduce the influx of monocytes and the activation of macrophages in the myocardium, resulting in mitigation of cardiac hypertrophy and dysfunction [32]. Additionally, the proinflammatory and antiangiogenic effect of Tregs played an essential role in the progression of immune activation and pathological left ventricular remodeling. Restoration of proper Treg function may be a promising approach to therapeutic immunomodulation in HF [33]. Based on the immune-related functions results, type I IFN infiltrated higher in HF group. Previous study revealed that through initiation of the STING-IRFs-type I IFN signaling cascade, The cGAS/STING pathway is associated with the early inflammatory response during pressure overload-induced HF [34].

In addition, the two diagnostic markers are correlated with immune response. FCN3 is a pattern-recognition molecule with the ability to activate the lectin pathway of complement. Low FCN3 levels were intimately related to increased complement activation product C3a and accordingly decreased concentrations of complement C3 [35]. Tissue injury, fibrosis, and inflammation are tightly interwoven processes. SPARC serves as a critical regulator of collagen processing and deposition. The interaction between SMOC2 and TGF-β1 in hepatocyte can modulate hepatic inflammation and fibrogenesis through the nuclear factor-κB signal pathway [36]. By analyzing the correlation between FCN3, SMOC2, and immune cells, it was found that FCN3 was negatively correlated with Mast cells, while there was positive correlation between SMOC2 and Mast cells. The bulk of evidence has shown that myocardial Mast cells exert a prominent role in HF pathogenesis. It can promote cardiac hypertrophy and fibrosis through the mechanism of releasing platelet-derived growth factor, proteases, and cytokines, which can induce cardiomyocyte hypertrophy and cardiac cell death [37].

Several limitations of our study should be admitted. Firstly, the study sample size was small due to low heart specimen numbers taken from HF patients. Secondly, molecular biology experiments, such as reverse transcription-polymerase chain reaction and western blotting, should be carried out to verify our bioinformatic findings. Thirdly, the concrete mechanism of FCN3 and SMOC2 in HF was obscure. Most importantly, our research was a retrospective investigation and further experiments are required to explore the detailed mechanisms through which FCN3 and SMOC2 regulate cellular responses in HF, as well as the role of immune infiltration in HF.

5. Conclusion

In summary, we constructed and validated a novel diagnostic signature of HF by combining RRA, WGCNA, and feature selection

methods. Besides, we found that immune infiltration plays a critical role in the onset and progression of HF. Our findings may provide promising targets for the treatment of HF. More studies should be carried out to verify our findings and clarify the fundamental mechanisms of immune infiltration in HF development.

Funding

This study was supported by the Doctoral Scientific Research Foundation of Liaoning Province, China (No. 2023-BS-034).

Ethical approval

Not applicable.

Informed consent

Not applicable.

Consent for publication

Not applicable.

CRediT authorship contribution statement

Dingyuan Tu: Writing – original draft, Methodology, Investigation, Data curation, Conceptualization. **Qiang Xu:** Software, Methodology, Data curation. **Xiaoli Zuo:** Writing – review & editing, Methodology, Investigation. **Chaoqun Ma:** Writing – review & editing, Formal analysis, Conceptualization.

Declaration of competing interest

The authors declare that they have no known competing financial interests or personal relationships that could have appeared to influence the work reported in this paper.

Acknowledgements

We all authors sincerely acknowledge the contributions from the GEO project. We also thank Home for Researchers (https://www.home-for-researchers.com/) for their linguistic assistance.

Appendix A. Supplementary data

Supplementary data to this article can be found online at https://doi.org/10.1016/j.ijcha.2024.101335.

References

[1] A. Gupta, Y. Yu, Q.i. Tan, S. Liu, F.A. Masoudi, X. Du, J. Zhang, H.M. Krumholz, J. Li, Quality of care for patients hospitalized for heart failure in China, JAMA Netw. Open 3 (1) (2020) e1918619, https://doi.org/10.1001/jamanetworkopen.2019.18619.

[2] S.M. Rego, M.P. Snyder, High throughput sequencing and assessing disease risk, Cold Spring Harb. Perspect. Med. 9 (1) (2019) a026849, https://doi.org/10.1101/cshperspect.a026849.

[3] P. Langfelder, S. Horvath, WGCNA: an R package for weighted correlation network analysis, BMC Bioinf. 9 (2008) 559, https://doi.org/10.1186/1471-2105-9-559.

[4] R. Kolde, S. Laur, P. Adler, J. Vilo, Robust rank aggregation for gene list integration and meta-analysis, Bioinformatics 28 (4) (2012) 573–580, https://doi.org/10.1093/bioinformatics/btr709.

[5] E. Martini, P. Kunderfranco, C. Peano, P. Carullo, M. Cremonesi, T. Schorn, R. Carriero, A. Termanini, F.S. Colombo, E. Jachetti, C. Panico, G. Faggian, A. Fumero, L. Torracca, M. Molgora, J. Cibella, C. Pagiatakis, J. Brummelman, G. Alvisi, E.M.C. Mazza, M.P. Colombo, E. Lugli, G. Condorelli, M. Kallikourdis, Single-cell sequencing of mouse heart immune infiltrate in pressure overload-driven heart failure reveals extent of immune activation, Circulation 140 (25) (2019) 2089–2107, https://doi.org/10.1161/CIRCULATIONAHA.119.041694.

[6] S.W. Kong, Y.W. Hu, J.W.K. Ho, S. Ikeda, S. Polster, R. John, J.L. Hall, E. Bisping, B. Pieske, C.G. dos Remedios, W.T. Pu, Heart failure-associated changes in RNA splicing of sarcomere genes, Circ. Cardiovasc. Genet. 3 (2) (2010) 138–146, https://doi.org/10.1161/CIRCGENETICS.109.904698.

[7] S. Greco, P. Fasanaro, S. Castelvecchio, Y. D'Alessandra, D. Arcelli, M. Di Donato, A. Malavazos, M.C. Capogrossi, L. Menicanti, F. Martelli, MicroRNA dysregulation in diabetic ischemic heart failure patients, Diabetes 61 (6) (2012) 1633–1641, https://doi.org/10.2337/db11-0952.

[8] M.M. Molina-Navarro, E. Roselló-Lletí, A. Ortega, E. Tarazón, M. Otero, L. Martínez-Dolz, F. Lago, J.R. González-Juanatey, F. España, P. García-Pavía, J. A. Montero, M. Portolés, M. Rivera, G. Gonzalez, Differential gene expression of cardiac ion channels in human dilated cardiomyopathy, PLoS One 8 (12) (2013) e79792, https://doi.org/10.1371/journal.pone.0079792.

[9] Y. Liu, M. Morley, J. Brandimarto, S. Hannenhalli, Y.u. Hu, E.A. Ashley, W.H. W. Tang, C.S. Moravec, K.B. Margulies, T.P. Cappola, M. Li, RNA-seq identifies novel myocardial gene expression signatures of heart failure, Genomics 105 (2) (2015) 83–89, https://doi.org/10.1016/j.ygeno.2014.12.002.

[10] E.H. Kim, V.I. Galchev, J.Y. Kim, S.A. Misek, T.K. Stevenson, M.D. Campbell, F. D. Pagani, S.M. Day, T.C. Johnson, J.G. Washburn, K.L. Vikstrom, D.E. Michele, D. E. Misek, M.V. Westfall, Differential protein expression and basal lamina remodeling in human heart failure, Proteomics Clin. Appl. 10 (5) (2016) 585–596, https://doi.org/10.1002/prca.201500099.

[11] S.J. Matkovich, B. Al Khiami, I.R. Efimov, S. Evans, J. Vader, A. Jain, B. H. Brownstein, R.S. Hotchkiss, D.L. Mann, Widespread Down-regulation of cardiac mitochondrial and sarcomeric genes in patients with sepsis, Crit. Care Med. 45 (3) (2017) 407–414, https://doi.org/10.1097/CCM.0000000000002207.

[12] M.E. Sweet, A. Cocciolo, D. Slavov, K.L. Jones, J.R. Sweet, S.L. Graw, T.B. Reece, A. V. Ambardekar, M.R. Bristow, L. Mestroni, M.R.G. Taylor, Transcriptome analysis of human heart failure reveals dysregulated cell adhesion in dilated cardiomyopathy and activated immune pathways in ischemic heart failure, BMC Genomics 19 (1) (2018), https://doi.org/10.1186/s12864-018-5213-9.

[13] M.E. Ritchie, B. Phipson, D.i. Wu, Y. Hu, C.W. Law, W. Shi, G.K. Smyth, limma powers differential expression analyses for RNA-sequencing and microarray studies, Nucleic Acids Res. 43 (7) (2015) e47, https://doi.org/10.1093/nar/gkv007.

[14] G. Yu, L.G. Wang, Y. Han, Q.Y. He, clusterProfiler: an R package for comparing biological themes among gene clusters, OMICS 16 (5) (2012) 284–287, https://doi.org/10.1089/omi.2011.0118.

[15] M.M. Mukaka, Statistics corner: A guide to appropriate use of correlation coefficient in medical research, Malawi Med. J. 24 (3) (2012) 69–71.

[16] C.W. Tsao, A.W. Aday, Z.I. Almarzooq, A. Alonso, A.Z. Beaton, M.S. Bittencourt, A. K. Boehme, A.E. Buxton, A.P. Carson, Y. Commodore-Mensah, M.S.V. Elkind, K. R. Evenson, C. Eze-Nliam, J.F. Ferguson, G. Generoso, J.E. Ho, R. Kalani, S.S. Khan, B.M. Kissela, K.L. Knutson, D.A. Levine, T.T. Lewis, J. Liu, M.S. Loop, J. Ma, M. E. Mussolino, S.D. Navaneethan, A.M. Perak, R. Poudel, M. Rezk-Hanna, G.A. Roth, E.B. Schroeder, S.H. Shah, E.L. Thacker, L.B. VanWagner, S.S. Virani, J.H. Voecks, N.-Y. Wang, K. Yaffe, S.S. Martin, Heart disease and stroke Statistics-2022 update: a report from the American Heart Association, Circulation 145 (8) (2022), https://doi.org/10.1161/CIR.0000000000001052.

[17] S. Liang, A. Ma, S. Yang, Y. Wang, Q. Ma, A review of matched-pairs feature selection methods for gene expression data analysis, Comput. Struct. Biotechnol. J. 16 (2018) 88–97, https://doi.org/10.1016/j.csbj.2018.02.005.

[18] K.N. Bachmann, D.K. Gupta, M. Xu, E. Brittain, E. Farber-Eger, P. Arora, et al., Unexpectedly low natriuretic peptide levels in patients with heart failure, JACC Heart Fail. 9 (3) (2021) 192–200, https://doi.org/10.1016/j.jchf.2020.10.008.

[19] U. Holmskov, S. Thiel, J.C. Jensenius, Collections and ficolins: humoral lectins of the innate immune defense, Annu. Rev. Immunol. 21 (2003) 547–578, https://doi.org/10.1146/annurev.immunol.21.120601.140954.

[20] I. Shi, N. Hashemi Sadraei, Z.H. Duan, T. Shi, Aberrant signaling pathways in squamous cell lung carcinoma, Cancer Inform. 10 (2011) 273–285, https://doi.org/10.4137/CIN.S8283.

[21] J.-H. Luo, B. Ren, S. Keryanov, G.C. Tseng, U.N.M. Rao, S.P. Monga, S. Strom, A. J. Demetris, M. Nalesnik, Y.P. Yu, S. Ranganathan, G.K. Michalopoulos, Transcriptomic and genomic analysis of human hepatocellular carcinomas and hepatoblastomas, Hepatology 44 (4) (2006) 1012–1024, https://doi.org/10.1002/hep.21328.

[22] A. Szala, S. Sawicki, A.S. Swierzko, J. Szemraj, M. Sniadecki, M. Michalski, A. Kaluzynski, J. Lukasiewicz, A. Maciejewska, D. Wydra, D.C. Kilpatrick, M. Matsushita, M. Cedzynski, Ficolin-2 and ficolin-3 in women with malignant and benign ovarian tumours, Cancer Immunol. Immunother. 62 (8) (2013) 1411–1419, https://doi.org/10.1007/s00262-013-1445-3.

[23] S.J. Catarino, F.A. Andrade, L. Bavia, L. Guilherme, I.J. Messias-Reason, Ficolin-3 in rheumatic fever and rheumatic heart disease, Immunol. Lett. 229 (2021) 27–31, https://doi.org/10.1016/j.imlet.2020.11.006.

[24] C.-E. Fernandez-García, E. Burillo, J.S. Lindholt, D. Martinez-Lopez, K. Pilely, C. Mazzeo, J.-B. Michel, J. Egido, P. Garred, L.M. Blanco-Colio, J.L. Martin-Ventura, Association of ficolin-3 with abdominal aortic aneurysm presence and progression, J. Thromb. Haemost. 15 (3) (2017) 575–585, https://doi.org/10.1111/jth.13608.

[25] T. Peeters, S. Monteagudo, P. Tylzanowski, F.P. Luyten, R. Lories, F. Cailotto, C. Zhang, SMOC2 inhibits calcification of osteoprogenitor and endothelial cells, PLoS One 13 (6) (2018) e0198104, https://doi.org/10.1371/journal.pone.0198104.

[26] L.i. Luo, C.-C. Wang, X.-P. Song, H.-M. Wang, H. Zhou, Y. Sun, X.-K. Wang, S. Hou, F.-Y. Pei, Suppression of SMOC2 reduces bleomycin (BLM)-induced pulmonary fibrosis by inhibition of TGF-β1/SMADs pathway, Biomed. Pharmacother. 105 (2018) 841–847, https://doi.org/10.1016/j.biopha.2018.03.058.

[27] H. Mommaerts, C.V. Esguerra, U. Hartmann, F.P. Luyten, P. Tylzanowski, Smoc2 modulates embryonic myelopoiesis during zebrafish development, Dev. Dyn. 243 (11) (2014) 1375–1390, https://doi.org/10.1002/dvdy.24164.
[28] C. Xin, J. Lei, Q. Wang, Y. Yin, X. Yang, J.A. Moran Guerrero, V. Sabbisetti, X. Sun, V.S. Vaidya, J.V. Bonventre, Therapeutic silencing of SMOC2 prevents kidney function loss in mouse model of chronic kidney disease, iScience. 24 (10) (2021) 103193, https://doi.org/10.1016/j.isci.2021.103193.
[29] S. Morkmued, F. Clauss, B. Schuhbaur, V. Fraulob, E. Mathieu, J. Hemmerlé, H. Clevers, B.-K. Koo, P. Dollé, A. Bloch-Zupan, K. Niederreither, Deficiency of the SMOC2 matricellular protein impairs bone healing and produces age-dependent bone loss, Sci. Rep. 10 (1) (2020), https://doi.org/10.1038/s41598-020-71749-6.
[30] E. Forte, B. Perkins, A. Sintou, H.S. Kalkat, A. Papanikolaou, C. Jenkins, M. Alsubaie, R.A. Chowdhury, T.M. Duffy, D.A. Skelly, J. Branca, M. Bellahcene, M. D. Schneider, S.E. Harding, M.B. Furtado, F.S. Ng, M.G. Hasham, N. Rosenthal, S. Sattler, Cross-priming dendritic cells exacerbate immunopathology after ischemic tissue damage in the heart, Circulation 143 (8) (2021) 821–836, https://doi.org/10.1161/CIRCULATIONAHA.120.044581.
[31] A. Ngkelo, A. Richart, J.A. Kirk, P. Bonnin, J. Vilar, M. Lemitre, et al., Mast cells regulate myofilament calcium sensitization and heart function after myocardial infarction, J. Exp. Med. 213 (7) (2016) 1353–1374, https://doi.org/10.1084/jem.20160081.
[32] Y. Wang, S. Sano, K. Oshima, M. Sano, Y. Watanabe, Y. Katanasaka, Y. Yura, C. Jung, A. Anzai, F.K. Swirski, N. Gokce, K. Walsh, Wnt5a-mediated neutrophil recruitment has an obligatory role in pressure overload-induced cardiac dysfunction, Circulation 140 (6) (2019) 487–499, https://doi.org/10.1161/CIRCULATIONAHA.118.038820.
[33] S.S. Bansal, M.A. Ismahil, M. Goel, G. Zhou, G. Rokosh, T. Hamid, S.D. Prabhu, Dysfunctional and proinflammatory regulatory T-lymphocytes are essential for adverse cardiac remodeling in ischemic cardiomyopathy, Circulation 139 (2) (2019) 206–221, https://doi.org/10.1161/CIRCULATIONAHA.118.036065.
[34] D. Hu, Y.-X. Cui, M.-Y. Wu, L. Li, L.-N. Su, Z. Lian, H. Chen, Cytosolic DNA sensor cGAS plays an essential pathogenetic role in pressure overload-induced heart failure, Am. J. Phys. Heart Circ. Phys. 318 (6) (2020) H1525–H1537.
[35] Z. Prohászka, L. Munthe-Fog, T. Ueland, T. Gombos, A. Yndestad, Z. Förhécz, M.-O. Skjoedt, Z. Pozsonyi, A. Gustavsen, L. Jánoskuti, I. Karádi, L. Gullestad, C. P. Dahl, E.T. Askevold, G. Füst, P. Aukrust, T.E. Mollnes, P. Garred, R.B. Sim, Association of ficolin-3 with severity and outcome of chronic heart failure, PLoS One 8 (4) (2013) e60976, https://doi.org/10.1371/journal.pone.0060976.
[36] Y. Yuting, F. Lifeng, H. Qiwei, Secreted modular calcium-binding protein 2 promotes high fat diet (HFD)-induced hepatic steatosis through enhancing lipid deposition, fibrosis and inflammation via targeting TGF-β1, Biochem. Biophys. Res. Commun. 509 (1) (2019) 48–55, https://doi.org/10.1016/j.bbrc.2018.12.006.
[37] X. Liu, G.P. Shi, J. Guo, Innate immune cells in pressure overload-induced cardiac hypertrophy and remodeling, Front. Cell Dev. Biol. 9 (2021) 659666, https://doi.org/10.3389/fcell.2021.659666.